# Design and Characterization of Heteroleptic Ruthenium Complexes Containing Benzimidazole Ligands for Dye-Sensitized Solar Cells: The Effect of Thiophene and Alkyl Substituents on Photovoltaic Performance

Wei-Kai Huang, Hui-Ping Wu, Pi-Lun Lin, and Eric Wei-Guang Diau*

Department of Applied Chemistry and Institute of Molecular Science, National Chiao Tung University, Hsinchu 30010, Taiwan

Ⓢ *Supporting Information*

ABSTRACT: We designed heteroleptic ruthenium complexes **RD16−RD18** containing fluoro-substituted and thiophene-based benzimidazole ligands for dye-sensitized solar cells. Whereas the substitution of only fluorine in the **RD12** device has an effect of enhancing the open-circuit voltage (V_{OC}), additional substitution of thiophene in the **RD16−RD18** sensitizers showed a slightly decreased V_{OC}. Systematic enhanced short-circuit current density (J_{SC}) and efficiency (η) of power conversion of the devices had the order **RD18 > RD17 > RD16 > RD12 > N719**, attributed to the increasing light-harvesting ability and the broadened spectral features with thiophene-based ligands. Measurements of charge extraction and intensity-modulated photovoltage spectra indicate that thiophene substitution shifts downward the TiO_2 potential and accelerates charge recombination, but inclusion of a long hexyl chain on the thiophene moiety retards charge recombination to account for the variation of V_{OC} in the series. For a duration test of device performance at ambient temperature, only ~2% degradation of cell performance was found for the devices of **RD18** and **RD12** over 2000 h, but a 10% decrease in overall efficiency was observed in the **N719** device.
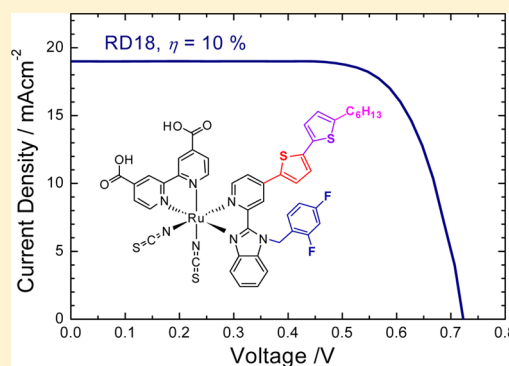
■ INTRODUCTION

Dye-sensitized solar cells (DSSCs) attract considerable attention because of their potential as next-generation photovoltaic devices.[1,2] Photosensitizers such as ruthenium complexes,[3,4] zinc porphyrin,[5−8] and metal-free organic dyes[9−11] have been developed to serve as efficient harvesters of light for DSSC. The DSSC devices made of homoleptic ruthenium complexes (e.g., **N3** and **N719**) attained an impressive efficiency, η ~11%, of power conversion under one-sun illumination,[12,13] but the enduring stability of the devices made of these complexes has become a major challenge; an amphiphilic Ru sensitizer (**Z907**) was developed to improve their durability.[14,15] The strategy for design of the **Z907** dye is to replace one bidentate 4,4′-dicarboxylic-2,2′-bipyridine (dcbpy) ligand in the **N3** dye with an ancillary ligand similar to dcbpy but with two identical long alkyl chains replacing the two carboxylic acid groups.[16] Although the stability of the **Z907** device was significantly improved, the dye suffers from small absorptivity to promote further its cell performance. To improve the light-harvesting efficiency via an enhanced absorption coefficient, heteroleptic ruthenium complexes were developed with various thiophene-based ancillary ligands.[17−26] Similar to the molecular design for a **Z907** dye, the two long alkyl chains in the ancillary ligand were replaced with two identical thiophene derivatives in the thiophene-based heteroleptic Ru complexes. These thiophene derivatives feature

excellent light-harvesting abilities as photosensitizers (such as **C101** and **C106** dyes), so to achieve remarkable efficiencies of power conversion, above 11.5%.[22−24]

For our designed heteroleptic ruthenium complexes containing benzimidazole (BI) ligands, the cell performance of the best dye (**RD5**) in the series was comparable to that of a **N719** dye.[27] This promising result encouraged us to design BI-based heteroleptic Ru dyes in a new series with the ancillary ligand consisting of a bidentate pyridine-benzimidazole moiety that is readily modified in four substitutable positions.[28] These fluoro-substituted devices effectively raise the TiO_2 potential and retard the charge recombination for an enhanced open-circuit voltage (V_{OC}) with increasing number of fluorine atoms, but the corresponding short-circuit current density (J_{SC}) values show an opposite trend.[28] Although the best dye (**RD12**) in the series exhibited a device performance superior to that of a **N719** device, the molar absorption coefficients of these dyes are smaller than that of **N719**, which limits their light-harvesting ability to enhance the device performance. As examples[17−26,29,30] including thiophene derivatives in the design of heteroleptic Ru dyes to enhance their light-harvesting capabilities were successful, in the present work we further
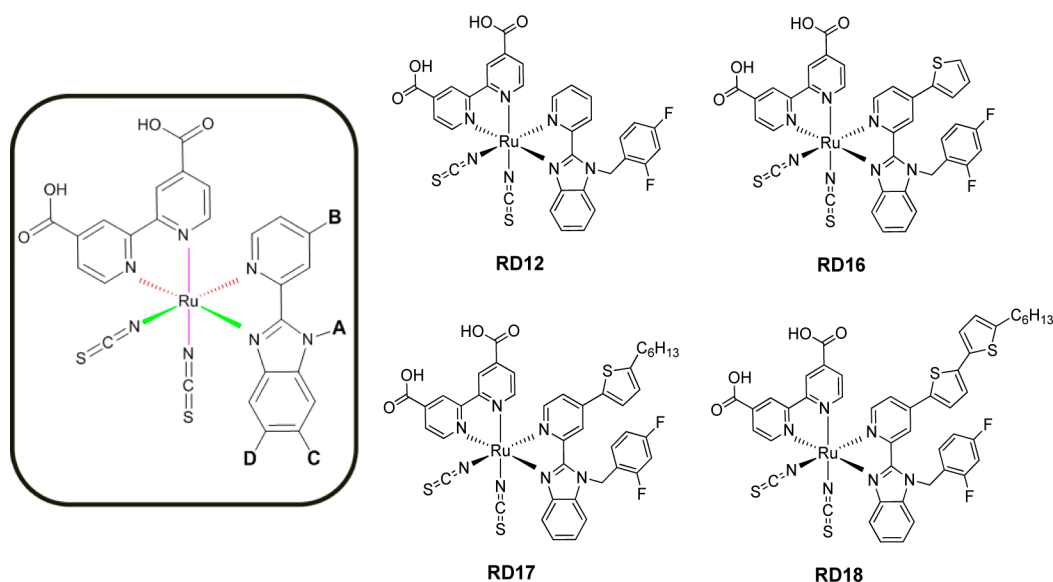
Chart 1. Molecular Design of a Heteroleptic Ruthenium Complex Containing the Benzimidazole Ligand with Possible Substitutions in the A, B, C, and D Positions and Molecular Structures of RD12, RD16, RD17, and RD18 Reported Herein

modified position **B** in the pyridine part of the ancillary ligand with thiophene derivatives based on the structure of **RD12**.[28]

As shown in Chart 1, **RD16** has only one thiophene unit substituted in the **B** position. In **RD17** a hexyl chain is attached in the α-position of the thiophene group, making half of the ligand resemble **C101** but the other half retained as in **RD12**. In **RD18**, a further thiophene group is added in the pyridine part of the ligand; this alkyl bithiophene substitute resembles half of the ancillary ligand in the **CYC-B1** dye[17] for an exceptional light-harvesting capacity. The present work continues our systematic investigation of BI-based Ru sensitizers to promote the light-harvesting ability of the dyes with thiophene substituents to achieve outstanding device performance. Such a molecular design shows a systematic trend of cell performance with the order **RD18 > RD17 > RD16 > RD12 > N719**. We measured charge extraction (CE) and intensity-modulated photovoltage spectra (IMVS) to understand the trend of device performance in this series. Upon optimization, the device made of **RD18** yielded J_{SC}/mA cm^{-2} = 17.80, V_{OC}/mV = 735, FF = 0.73, and η = 9.6%, which is significantly greater than that of an N719 device, η = 8.8%, similarly fabricated. A test of storage over 2000 h near 295 K indicated almost no degradation of performance for the devices of **RD18** and **RD12** but a 10% loss of efficiency in the N719 device.

■ EXPERIMENTAL SECTION

Synthesis. The syntheses of **RD16−RD18** were similar to that of **RD12** except that 4-bromopyridine-2-carboxylic acid was a starting material instead of picolinic acid to prepare the bromo-substituted BI precursor (**a**) and that additional Stille coupling reactions were involved to make the ancillary ligands **L16−L18**. The details of synthetic procedures and the corresponding molecular characterizations follow.

2-(4-Bromopyridin-2-yl)benzimidazole (a). 4-Bromopyridine-2-carboxylic acid (1.40g, 7 mmol), 1,2-benzenediamine (0.8g, 7.7 mmol), and PPA (10 g) were heated to 150 °C for 3 h. After cooling, the solution was poured into cool water with stirring; the pH was adjusted to 7−8 on addition of NaOH; the

resulting light yellow precipitate was filtered, washed with water, and dried in air without further purification.

2-(4-Bromopyridin-2-yl)-1-(2,4-difluorobenzyl)-benzimidazole (b). 2-(4-Bromopyridin-2-yl)benzimidazole (**a**) (0.67 g, 2.4 mmol) and K$_2$CO$_3$ (0.69 g, 5 mmol) were dissolved in DMF (20 mL) and stirred for 30 min; 1-(bromomethyl)-2,4-difluorobenzene (0.50g, 2.9 mmol) was added to the reaction mixture that was then stirred at 295 K for 4 h. After evaporation of the solvent under decreased pressure, H$_2$O (50 mL) and ethyl acetate (50 mL) were added. The organic layer was separated and dried over MgSO4. The crude product was purified on a column chromatograph (silica gel) with a mixture of ethyl acetate and hexane (1/4) as eluent to afford a white precipitate (0.71g, 74.1%). ^{1}H NMR (DMSO-d_6): 8.56−8.52 (m, 2H), 7.80 (m, 2H), 7.60 (m, 1H), 7.60 (t, 1H), 7.36−7.21 (m, 3H), 6.93−6.90 (t, 2H), 6.22 (s, 2H). Mass, ESI-MS: calcd *m/z* 399; found 398.8 [M − H]$^-$.

Ligands. *1-(2,4-Difluorobenzyl)-2-(4-(thiophen-2-yl)-pyridin-2-yl)-benzimidazole (L16).* 2-(4-Bromopyridin-2-yl)-1-(2,4-difluorobenzyl)benzimidazole (**b**) (0.4 g, 1 mmol), trimethyl(thiophen-2-yl)stannane (0.3 g, 1.2 mmol), and Pd(PPh$_3$)$_4$ (0.06 g, 0.05 mmol) were dissolved in dry DMF stirred at 85 °C under Ar overnight. After rotary evaporation of DMF, the resulting solid was purified on a column chromatograph (silica gel) with a mixture of ethyl acetate and hexane (1/4) as eluent to afford a yellow/white precipitate (0.28 g, 74.7%). ^{1}H NMR (DMSO-d_6): 8.65 (d, 1H), 8.52 (d, 1H), 7.96 (d, 1H), 7.84−7.78 (m, 3H), 7.62−7.59 (m, 1H), 7.34−7.24 (m, 4H), 6.93−6.89 (m, 2H), 6.24 (s, 2H). Mass, ESI-MS: calcd *m/z* 375; found 373.9 [M − H]$^-$.

1-(2,4-Difluorobenzyl)-2-(4-(5-hexylthiophen-2-yl)pyridin-2-yl)benzimidazole (L17). 2-(4-Bromopyridin-2-yl)-1-(2,4-difluorobenzyl)benzimidazole (**b**) (0.24 g, 0.6 mmol), (5-hexylthiophen-2-yl)trimethylstannane(0.3 g, 0.9 mmol), and Pd(PPh$_3$)$_4$ (0.04 g, 0.03 mmol) were dissolved in dry DMF stirred at 85 °C under Ar overnight. After rotary evaporation of DMF, the resulting solid was purified on a column chromatograph (silica gel) with a mixture of ethyl acetate and hexane (1/5) as eluent to afford a yellow/white precipitate (0.21 g, 71.9%). ^{1}H NMR (DMSO-d_6): 8.45 (d, 1H), 7.83−7.78 (m,

2H), 7.71 (t, 1H), 7.60 (t, 1H), 7.35−7.22 (m, 3H), 7.00−6.89 (m, 3H), 6.24 (s, 2H), 2.69 (t, 2H), 1.70−1.61 (m, 2H), 1.35−1.23 (m, 6H), 0.85 (t, 3H). Mass, ESI-MS: calcd *m/z* 487; found 486.2 [M − H]⁻.

1-(2,4-Difluorobenzyl)-2-(4-(5-(5-hexylthiophen-2-yl)-thiophen-2-yl)pyridin-2-yl)benzimidazole (L18). 2-(4-Bromo-pyridin-2-yl)-1-(2,4-difluorobenzyl)benzimidazole (**b**) (0.4 g, 1 mmol), (5-(5-hexylthiophen-2-yl)thiophen-2-yl)-trimethylstannane (0.62 g, 1.5 mmol), and Pd(PPh₃)₄ (0.06 g, 0.05 mmol) were dissolved in dry DMF stirred at 85 °C under Ar overnight. After rotary evaporation of DMF, the resulting solid was purified on a column chromatograph (silica gel) with a mixture of ethyl acetate and hexane (1/6) as eluent to afford yellow precipitate (0.37 g, 65.0%). ¹H NMR (DMSO-*d₆*): 8.65 (d, 1H), 8.50 (d, 1H), 7.92 (d, 1H), 7.84−7.77 (m, 2H), 7.60 (t, 1H), 7.38−7.23 (m, 5H), 6.94−6.87 (m, 3H), 6.25 (s, 2H), 2.81 (t,2H), 1.64 (t, 2H), 1.35−1.22 (m, 6H), 0.87 (t, 3H) Mass, ESI-MS: calcd *m/z* 569; found 568.1 [M − H]⁻.

Complexes. The ¹HNMR spectra of the **RD16-RD18** dyes are shown in Figure S1, Supporting Information. The NMR spectra of **RD** series dyes are complex because they contain two stereoisomers that cannot be separated by using the column chromatography methods such as silica gel, aluminum oxide, or Sephadex LH-20. As a result, the NMR spectra exhibit groups of doublet/multiple peaks in the 5−10 ppm region. Integration of the spectral peaks gives the ratio of the two isomers close to 1:1.[28] Therefore, the average effect of the two inseparable stereoisomers should be considered for the results discussed in the following.

[Ru(4,4′-dicarboxylic-2,2′-bipyridine)(1-(2,4-difluoroben-zyl)-2-(4-(thiophen-2-yl)pyridin-2-yl)-benzimidazole)NCS2] (RD16). In a typical one-pot synthesis, [RuCl₂(*p*-cymene)]₂ (153 mg, 0.25 mmol) was dissolved in DMF (20 mL), and the precursor ligand **L16** (188 mg, 0.5 mmol) was added. The reaction mixture was heated at 80 °C under argon for 4 h; then dcbpy (122 mg, 0.5 mmol) was added. The reaction mixture was refluxed at 140 °C for another 4 h in darkness to avoid photoinduced cis−trans isomerization. Excess KNCS was added to the reaction mixture that was heated at 140 °C for 5 h. After the reaction, the solvent was removed with a rotary evaporator. Water was added to the resulting mixture to remove excess KNCS. The water-insoluble product was then collected on a sintered-glass crucible with suction filtration, washed with distilled water followed by diethyl ether, and dried in air. The crude product was dissolved in methanol and then passed through a column (Sephadex LH-20) with methanol as eluent. The main band was collected and concentrated. This purification was repeated five times. A few drops of HNO₃ (aq, 0.01 M) were added to precipitate the purple red product (206 mg, 61.2%). Elemental analysis (%) calcd for C₃₇H₂₃N₇F₂O₄S₃Ru·0.5TBAOH·2.5H₂O: C 52.44, H 4.45, N 10.19; found: C 52.32, H 4.45, N 10.11. Mass, ESI-MS: calcd *m/z* 865.0; found *m/z* 864.3 [M − H]⁻.

[Ru(4,4′-dicarboxylic-2,2′-bipyridine)(1-(2,4-difluoroben-zyl)-2-(4-(5-hexylthiophen-2-yl)pyridin-2-yl)benzimidazole)-NCS2] (RD17). **RD17** was synthesized in a typical one-pot reaction with the same procedure as **RD16**. The reactants were [RuCl₂(*p*-cymene)]₂ (153 mg, 0.25 mmol), **L17** (243 mg, 0.5 mmol), dcbpy (122 mg, 0.5 mmol), and excess KNCS. The crude product was purified on a column (Sephadex LH-20) with methanol as eluent. The main band was collected and concentrated. This purification was repeated five times. A few

drops of HNO₃ (aq, 0.01M) were added to precipitate the purple red product (247 mg, 52.1%). Elemental analysis (%) calcd for C₄₃H₃₄N₇F₂O₄S₃Ru·0.5TBAOH·2H₂O·0.5MeOH: C 54.23, H 4.91, N 9.50; found: C 54.30, H 4.97, N 9.55. Mass, ESI-MS: calcd *m/z* 949.09; found *m/z* 949.4 [M − H]⁻.

[Ru(4,4′-dicarboxylic-2,2′-bipyridine)(1-(2,4-difluoroben-zyl)-2-(4-(5-(5-hexylthiophen-2-yl)-thiophen-2-yl)pyridin-2-yl)benzimidazole)NCS2] (RD18). **RD18** was synthesized in a typical one-pot reaction with the same procedure as **RD16**. The reactants were [RuCl₂(p-cymene)]₂ (153 mg, 0.25 mmol), **L18** (285 mg, 0.5 mmol), dcbpy (122 mg, 0.5 mmol), and excess KNCS. The crude product was purified on a column (Sephadex LH-20) with methanol as eluent. The main band was collected and concentrated. This purification was repeated five times. A few drops of HNO3 (aq, 0.01M) were added to precipitate the purple red product (274 mg, 53.2%). Elemental analysis (%) calcd for C₄₇H₃₇N₇F₂O₄S₄Ru·0.5TBAOH·1.5H₂O. MeOH: C 55.13, H 5.16, N 8.61; found: C 55.28, H 5.24, N 8.91 Mass, ESI-MS: calcd *m/z* 1031.08; found *m/z* 1030.3 [M − H]⁻.

■ CHARACTERIZATIONS

Electrochemical Measurements. Electrochemical tests were performed with a three-electrode potentiostat (CHI621D, CH Instruments) in dry DMF in the presence of (*n*-C₄H₉)₄NPF₆ (0.1 M). For cyclic voltammetry (CV) measurements, a three-electrode cell was equipped with a platinum (0.02 cm²) disk as working electrode, a platinum wire as auxiliary electrode, and an Ag wire as reference electrode. Potentials are reported vs Ag wire with reference to a ferrocene/ferrocenium (Fc/Fc⁺).

Electrode Preparation and Device Fabrication. Photo-anodes composed of nanocrystalline TiO₂ were prepared using the sol−gel method. A paste composed of TiO₂ nanoparticles (diameter ∼25 nm) and nanorods (length 100−300 nm and diameter 20−30 nm) for the transparent active layer was coated on a TiCl₄-treated and AR-coated FTO glass substrate (FTO, 8Ω/□) with repetitive screen printing to obtain the required thickness of the film. To improve the performance of the DSSC, an additional scattering layer (particle size 200−600 nm) was screen-printed on the transparent active layer. The TiO₂ working electrodes were gradually heated according to a programmed procedure: (1) heating at 80 °C for 15 min; (2) heating at 135 °C for 10 min; (3) heating at 325 °C for 30 min; (4) heating at 375 °C for 5 min; (5) heating at 450 °C for 15 min; (6) heating at 500 °C for 15 min. The resulting film comprised a transparent layer (thickness 17 *µ*m) and a scattering layer (thickness ∼5 *µ*m), which were treated again with TiCl₄ at 70 °C for 30 min and sintered at 500 °C for 30 min. After cooling in air, the sintered TiO₂ films were immersed in dye solutions (0.3 mM in anhydrous CH3CN/*t*-BuOH (1:1 v/v) at 25 °C for 3 h) containing CDCA (0.3 mM) for dye loading onto the working electrodes. The counter electrode was made on spin-coating the H₂PtCl₆/isopropyl alcohol solution onto a FTO glass substrate (FTO, 8Ω/□, typical size 1.0 × 1.5 cm²) through thermal decomposition at 380 °C for 30 min. The two electrodes were assembled into a cell of sandwich type and sealed with a hot-melt film (SX1170, thickness 25 *µ*m). Silver was coated on both electrodes to decrease the series resistance of the device. The electrolyte solution contained 1-methyl-3-propylimidazolium iodide (PMII, 1.0 M), guanidi-nium thiocyanate (GuSCN, 0.1 M), LiI (0.1 M), I₂ (0.03 M), and 4-*t*-butylpyridine (TBP, 0.5 M) in a solvent mixture containing acetonitrile and valeronitrile (volume ratio 85:15).

Scheme 1. Syntheses of Compounds (a) and (b), Benzimidazole Ligands L16-L18, and Ruthenium Complexes RD16-RD18
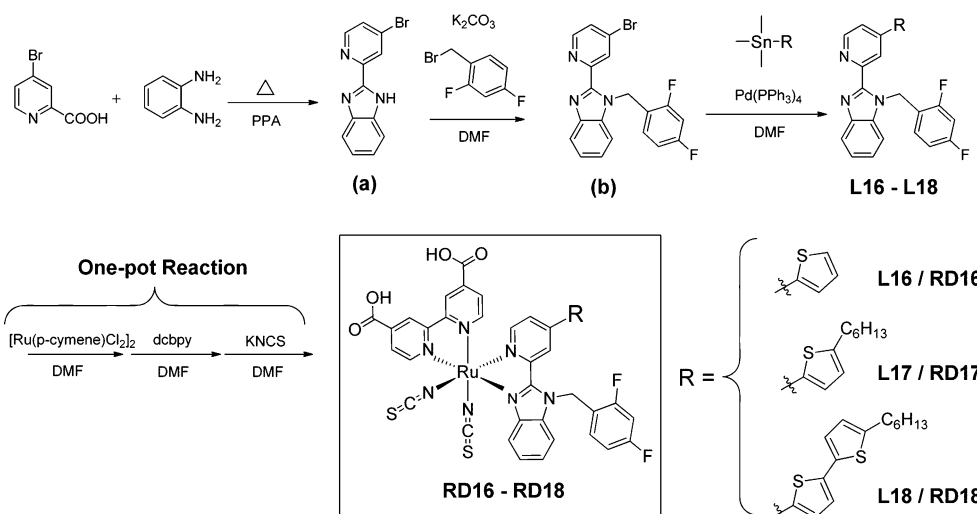
The reference ruthenium complex **N719** was purchased from solaronix, and before preparing dye solution, Sephadex LH-20 column purification with H_2O (with 2 equiv TBAOH) as an eluent was repeated five times. A few drops of HNO_3 (aq, 0.01M) were added to precipitate the final compound at pH lowered to 4.3.

Photovoltaic Characterization. The current−voltage characteristics were determined with a digital source meter (Keithley 2400) with the device under one-sun AM 1.5G irradiation from a solar simulator (XES-502S, SAN-EI) calibrated with a standard silicon reference cell (Oriel PN 91150 V, VLSI standards). The efficiency (η) of conversion of light to electricity is obtained via $\eta = J_{SC}V_{OC}FF/P_{in}$, in which J_{SC}/mA cm^{-2} is the current density measured at short circuit and V_{OC}/V is the voltage measured at open circuit. P_{in} is the input radiation power (for one-sun illumination P_{in} = 100 mW cm^{-2}), and FF is the fill factor. The spectra of the IPCE of the corresponding devices were recorded with a system comprising a Xe lamp (PTi A-1010, 150 W), a monochromator (PTi, 1200 g mm^{-1} blazed at 500 nm), and a source meter (Keithley 2400). A standard Si photodiode (ThorLabs FDS1010) served as reference to calibrate the power density of the light source at each wavelength.

Impedance Characterization. The intensity-modulated photovoltage spectra (IMVS) were measured with the CIMPS equipment (Zahner) at an open-circuit condition based on a red LED light (λ = 610 nm) at five intensities (1.5−30 mW cm^{-2}) controlled with a slave system (XPOT, Zahner) to obtain the photovoltaic response induced by the modulated light.[31] The modulated light was driven with a 10% ac perturbation current superimposed on a dc current in a frequency range from 0.1 to 1000 Hz. The measurements of charge extraction (CE) were performed with the same CIMPS system under the same bias light irradiations. For that experiment, the system was initially set to an open-circuit condition for 10 s for the photovoltage of the device to attain a steady state; the red light from the LED was then terminated while the device was simultaneously switched to a short-circuit condition to extract the charges generated at that bias light intensity.

■ RESULTS AND DISCUSSION

Scheme 1 summarizes the syntheses of **RD16−RD18**, which are similar to that of **RD12** except that 4-bromopyridine-2-carboxylic acid instead of picolinic acid became a starting material to prepare the bromo-substituted BI precursor (a) and that additional Stille coupling reactions[32] were undertaken to make ancillary ligands **L16−L18**.

Figure 1 compares the absorption spectra of these dyes with those of **N719**, **Z907**, and **C101**; the corresponding spectral
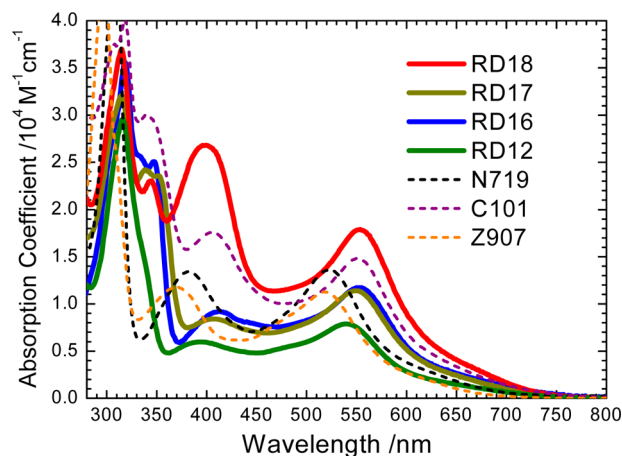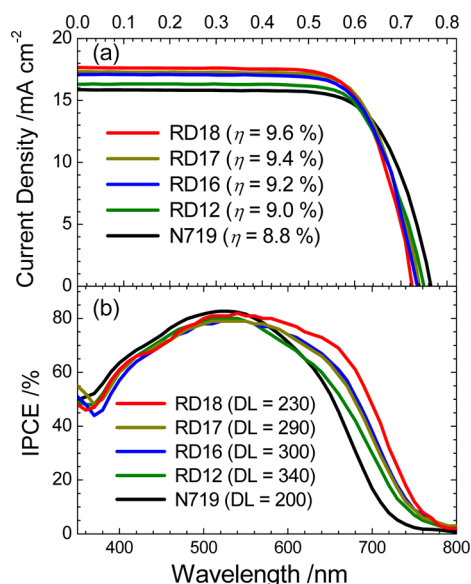

Figure 1. Absorption spectra of **RD12**, **RD16**, **RD17**, and **RD18** in DMF. The spectra of **N719**, **C101**, and **Z907** are shown as thin dashed curves for comparison.

and electrochemical data are summarized in Table S1, Supporting Information. Of two major features indicated in these spectra, thiophene substituents effectively enhanced the molar absorption coefficients for these dyes with a systematic order **RD18 > RD17 ∼ RD16 > RD12**, whereas the hexyl substitute plays scarcely any role in enhancing the absorption coefficients. The second feature is that substitution with thiophene derivatives effectively shifted the peak of the MLCT band toward the longer wavelength region with the extent of the red shift in an order **RD18 ∼ RD16 > RD17 > RD12**; the hexyl substituent plays only a minor role in the blue shift of the absorption features. The bathochromic spectral shifts of the **RD16−RD18** dyes relative to **N719** and **Z907** are

~30 nm, indicating the superior light-harvesting capability for dyes in this series. Moreover, with the same number of thiophene units in the ancillary ligand, the molar absorption coefficients of **RD18** are much greater than those of **C101** over the entire visible spectral region. This outstanding spectral feature makes **RD18** a promising candidate as a highly efficient photosensitizer for DSSC applications.

The electrochemical properties of compounds **RD12**, **RD16**−**RD18**, and **N719** were investigated with cyclic voltammetry (CV); the evaluated E_{HOMO} and E_{LUMO} values are listed in Table S1, Supporting Information. Figure S2 shows energy levels of the **RD** dyes for comparison of the HOMO/LUMO levels of each dye with respect to the conduction band (CB) of TiO_2 and the potential of the iodide/tri-iodide couple, which show that both electron injection and dye regeneration are feasible when they serve as photosensitizers for DSSC. These heteroleptic ruthenium dyes were fabricated into DSSC devices according to the same procedures with three identical TiO_2 films (thickness 17 + 5 μm). The current−voltage (J−V) measurements were performed under standard AM-1.5G illumination on devices with an active area 4 mm × 4 mm (0.16 cm^2) with a 5 mm × 5 mm (0.25 cm^2) black shadow mask.[33]

Figures 2a and 2b show typical current−voltage characteristics and the corresponding spectra of incident photon-to-

Figure 2. Photovoltaic properties: (a) current−voltage characteristics and (b) the corresponding IPCE action spectra of devices made of **RD12, RD16, RD17, RD18**, and **N719** with the same fabricated TiO_2 films (17 + 5 μm) and active area 0.16 cm^2 with 0.25 cm^2 black metal mask under one-sun AM-1.5G irradiation. The amounts of dye loading (DL) shown in (b) are in units of nmol cm^{-2}.

current conversion efficiency (IPCE), respectively, for the devices made of each ruthenium dye. Table 1 summarizes the amounts of dye-loading (DL) and the photovoltaic parameters. The photovoltaic performances of these devices show a systematic trend of J_{SC} but a variation of V_{OC} discussed below. For J_{SC}, the values increase with increasing number of thiophene units, showing an order **RD18** > **RD17** > **RD16** > **RD12** > **N719**. The enhancement of J_{SC} on alkyl substitution between **RD17** and **RD16** was insignificant; this result can be viewed from the variation of the IPCE action spectra showing a

Table 1. Photovoltaic Parameters of DSSC with Photosensitizers RD12, RD16−RD18, and N719 under Simulated AM-1.5G Illumination (Power 100 mW cm^{-2}) and Active Area 0.16 cm^2 with 0.25 cm^2 Black Shadow Mask

dye	dye-loading/nmol cm^{-2}	J_{SC}/ mA cm^{-2}	V_{OC}/ mV	FF	η/%
RD12	340	16.31	754	0.73	9.0
RD16	300	17.09	736	0.73	9.2
RD17	290	17.31	743	0.73	9.4
RD18	230	17.80	735	0.73	9.6
RD18[a]		18.93	734	0.72	10.0
N719	200	15.87	768	0.72	8.8

[a]Photovoltaic parameters of DSSC with **RD18** under AM-1.5G illumination (power 100 mW cm^{-2}) and active area 0.16 cm^2 without black shadow mask.

systematic trend with the breadth of the spectra in an order **RD18** > **RD16** ~ **RD17** > **RD12** > **N719**, consistent with their spectral features shown in Figure 1. Although the wavelengths of spectral features of the MLCT band are similar for the **RD16**−**RD18** dyes, the IPCE spectrum of **RD18** displays an ability to harvest light superior to that of other Ru dyes in the spectral range 550−700 nm; the IPCE values then gradually decrease to the background level near 800 nm. Even though less DL was involved in the **RD18** device, the significantly greater absorption coefficients of the dye play a key role to enhance J_{SC}.[17−26]

The V_{OC} values show an opposite trend of J_{SC}, with the order **N719** > **RD12** > **RD17** > **RD16** ~ **RD18**. This trend indicates that an involvement of the thiophene group in the BI ligand decreased the value of V_{OC}, but an additional long alkyl chain at the end of the thiophene group helped to promote V_{OC} slightly. The degradation of V_{OC} in the **RD16**−**RD18** devices was insignificant; the overall efficiencies of power conversion followed the trend of J_{SC} with the order **RD18** (η = 9.6%) > **RD17** (η = 9.4%) > **RD16** (η = 9.2%) > **RD12** (η = 9.0%) > **N719** (η = 8.8%). To understand the key factors affecting the trend of V_{OC}, we performed CE and IMVS measurements; the results are discussed below.

Figures 3a and 3b display plots of V_{OC} vs extracted charge densities (N_e) and electron lifetime (τ_R) vs N_e, respectively, for the five devices irradiated with red light from a LED (λ = 610 nm) at five intensities. The CE results (Figure 3a) indicate that the positions of the TiO_2 potentials of the devices have the order **N719** > **RD12** > **RD18** ~ **RD16** > **RD17**, whereas the IMVS results (Figure 3b) show the electron lifetimes of the devices to have the order **RD17** > **RD12** > **RD18** ~ **RD16** > **N719**. We understand that V_{OC} of **N719** is greater than that of the other **RD** dyes because of a significantly increased TiO_2 potential upon dye uptake for **N719** relative to other dyes, even though the rate of charge recombination in the case of **N719** is larger than those of the other dyes. The BI-based ancillary ligands hence have an effect of lowering the potential significantly but also retarding, to some extent, the charge recombination to compensate the loss of the potential decreases. With **RD12** as a reference, adding a thiophene unit in position **B** of the BI ligand lowers the potential and accelerates charge recombination, which reasonably explains the smaller V_{OC} for **RD16** than for **RD12**. Adding a further hexyl chain at the thiophene end of the ligand decreased slightly the potential but helps to retard the charge recombination to account for V_{OC} of **RD17** being larger than
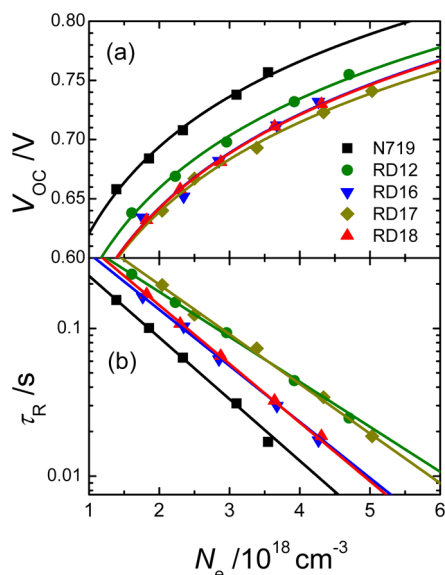
Figure 3. (a) Open-circuit voltage (V_{OC}) and (b) electron lifetimes (τ_R) as a function of extracted charge densities (N_e) for devices made of **RD12**, **RD16**−**RD18**, and **N719** irradiated with bias light at five intensities.

Figure 4. Stability of devices over 2000 h near 295 K showing the variation of the photovoltaic performance for (a) open-circuit voltage (V_{OC}), (b) short-circuit current density (J_{SC}), (c) fill factor (FF), and (d) efficiency (η) of power conversion for the devices made of **RD18**, **RD12** and **N719**.

that of **RD16**. Adding a second thiophene unit into the ligand of **RD17** to form **RD18** slightly raised the potential but accelerated charge recombination, giving V_{OC} for **RD18** smaller than for **RD17**. Our results thus indicate that the alkyl chain and the thiophene units little affected the potential but affected the charge recombination in varied directions. The net effects of an additional long alkyl chain and of an additional thiophene unit are compromised to some extent so that the potentials and the electron lifetimes are well matched between the **RD18** and **RD16** devices to explain their almost identical V_{OC} values. Because of the effect of accelerated charge recombination for the thiophene substituent, we expect that further thiophene units in the BI ligand of the dye would speed the charge recombination so as to decrease V_{OC} and degrade the performance of the device.

As the **RD18** dye featured an excellent light-harvesting ability to enhance J_{SC} of the device with only slightly decreased V_{OC}, we continued to test the device stability for a period over 2000 h near room temperature (~295 K).[34] Figure 4 shows the photovoltaic parameters as a function of time for dyes **RD18**, **RD12,** and **N719**, with the optimized devices fabricated under the same conditions without a shadow mask. As shown in Figure 4, the performances of the three devices exhibit initially a normal trend, with the order **RD18** (η = 10.1%) > **RD12** (η = 9.5%) > **N719** (η = 9.4%), similar to the variation of J_{SC}. Up to 50 h, the efficiencies of all three devices increased rapidly with the same order **RD18** (η = 10.5%) > **RD12** (η = 9.8%) > **N719** (η = 9.7%). At this time, device **N719** attained its best performance, device **RD12** attained a stable point near its maximum performance, but the performance of device **RD18** was still increasing to its maximum value. After 50 h, the efficiencies of **N719** maintained ~9.5% during 100−300 h but decreased rapidly to 9.2% at 500 h, to 9.0% at 1000 h, and eventually to 8.8% at 2000 h. For **RD12**, the device performance attained its maximum, η = 9.9%, at 400 h and remained stable (η > 9.7%) from 500 to 2000 h. For **RD18**, the best device performance (η = 10.7%) appeared at 300 h; the efficiency decreased slightly to 10.5% at 500 h and remained
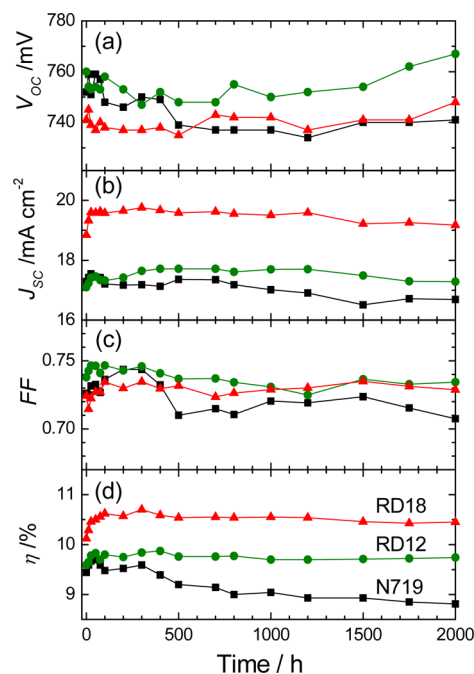
nearly constant at η ~10.5% until 2000 h. Although V_{OC} slightly increased at longer times for both **RD** devices, it decreased significantly for **N719**. As a result, V_{OC} displayed a trend **N719** ~ **RD12** > **RD18** at small durations but altered to the order **RD12** > **RD18** > **N719** at greater durations. The small decreases of J_{SC} of devices **RD18** and **RD12** are responsible for their efficiency degradation ~2%, but the degradation almost 10% of the **N719** device was accompanied by decreases of all three key photovoltaic parameters. Our results thus highlight the advantages of the **RD** series of photosensitizers not only for their superior photovoltaic performances but also for their outstanding durability for future commercialization.

■ CONCLUSION

We report herein the design, synthesis, and characterization of novel heteroleptic ruthenium complexes **RD16**−**RD18** containing thiophene-substituted benzimidazole ligands, with the molecular structures modified based on a fluoro-substituted Ru complex (**RD12**) reported elsewhere,[28] as promising photosensitizers for highly efficient dye-sensitized solar cells. Increasing the number of thiophene units in the BI ancillary ligands enhanced the light-harvesting ability to give J_{SC} and the corresponding IPCE of the devices with the order **RD18** > **RD17** ~ **RD16** > **RD12** > **N719**, consistent with their absorption spectral features. V_{OC} of the devices exhibited a trend opposite to that of J_{SC}, showing the order **N719** > **RD12** > **RD17** > **RD16** ~ **RD18**. The variation of V_{OC} is understood from the results of CE and IMVS measurements: the additional thiophene units seemed not to affect the potential much, but they accelerated the charge recombination to some extent; the additional alkyl chain shifted down the potential slightly but retarded the charge recombination significantly to account for the trend of V_{OC}. Because the decreases of V_{OC} for the thiophene-substituted dyes were insignificant, the overall device

2064

dx.doi.org/10.1021/jp3118693 | J. Phys. Chem. C 2013, 117, 2059−2065

performances display an order **RD18** > **RD17** > **RD16** > **RD12** > **N719**, similar to that of J_{SC}. The performances of the three typical devices, **RD18**, **RD12**, and **N719**, were further optimized with a complete thermal-pressure encapsulation for a test of stability over 2000 h near 295 K. For the best **RD18** device, its best performance was attained during 100−300 h, with a maximum, η = 10.7% (characterized without adding a shadow mask), at 300 h. Only ∼2% performance degradation was observed for both **RD12** and **RD18** devices, reflecting their excellent durability for future commercialization. Work is in progress to develop more efficient photosensitizers based on our BI-based ancillary ligands.

ASSOCIATED CONTENT

ⓈSupporting Information

Supplementary Figures S1−S4 and supplementary Table S1. This material is available free of charge via the Internet at http://pubs.acs.org.

AUTHOR INFORMATION

Corresponding Author

*E-mail: diau@mail.nctu.edu.tw. Fax: +886-3-5723764. Tel.: +886-3-5131524.

Notes

The authors declare no competing financial interest.

ACKNOWLEDGMENTS

REFERENCES

(1) Grätzel, M. *Acc. Chem. Res.* **2009**, *42*, 1788−1798.

(2) Hagfeldt, A.; Boschloo, G.; Sun, L.; Kloo, L.; Pettersson, H. *Chem. Rev.* **2010**, *110*, 6595−6663.

(3) Nazeeruddin, M. K.; Kay, A.; Rodicio, I.; Humphry-Baker, R.; Müller, E.; Liska, P.; Vlachopoulos, N.; Grätzel, M. *J. Am. Chem. Soc.* **1993**, *115*, 6382−6390.

(4) Robertson, N. *Angew. Chem., Int. Ed.* **2006**, *45*, 2338−2345.

(5) Imahori, H.; Umeyama, T.; Ito, S. *Acc. Chem. Res.* **2009**, *42*, 1809−1918.

(6) Martínez-Díaz, M. V.; de la Torre, G.; Torres, T. *Chem. Commun.* **2010**, *46*, 7090−7108.

(7) Yella, A.; Lee, H.-W.; Tsao, H. N.; Yi, C.; Chandiran, A. K.; Nazeeruddin, Md. K.; Diau, E. W.-G.; Yeh, C.-Y.; Zakeeruddin, S. M.; Grätzel, M. *Science* **2011**, *334*, 629−634.

(8) Li, L.-L.; Diau, E. W.-G. *Chem. Soc. Rev.* **2013**, *42*, 291−304.

(9) Zhang, G.; Bala, H.; Cheng, Y.; Shi, D.; Lv, X.; Yu, Q.; Wang, P. *Chem. Commun.* **2009**, 2198−2100.

(10) Ning, Z.; Tian, H. *Chem. Commun.* **2009**, 5483−5495.

(11) Ning, Z.; Fu, Y.; Tian, H. *Energy Environ. Sci.* **2010**, *3*, 1170−1181.

(12) Nazeeruddin, M. K.; De Angelis, F.; Fantacci, S.; Selloni, A.; Viscardi, G.; Liska, P.; Ito, S.; Takeru, B.; Grätzel, M. *J. Am. Chem. Soc.* **2005**, *127*, 16835−16847.

(13) Wang, Q.; Ito, S.; Grätzel, M.; Fabregat-Santiago, F.; Mora-Seró, I.; Bisquert, J.; Bessho, T.; Imai, H. *J. Phys. Chem. B* **2006**, *110*, 25210−25221.

(14) Wang, P.; Zakeeruddin, S. M.; Moser, J. E.; Nazeeruddin, Md. K.; Sekiguchi, T.; Grätzel, M. *Nat. Mater.* **2003**, *2*, 402−407.

(15) Wang, P.; Zakeeruddin, S. M.; Comte, P.; Charvet, R.; Humphry-Baker, R.; Grätzel, M. *J. Phys. Chem. B* **2003**, *107*, 14336−14341.

(16) Zakeeruddin, S. M.; Nazeeruddin, Md. K.; Humphry-Baker, R.; Péchy, P.; Quagliotto, P.; Barolo, C.; Viscardi, G.; Grätzel, M. *Langmuir* **2002**, *18*, 952−954.

(17) Chen, C.-Y.; Wu, S.-J.; Wu, C.-G.; Chen, J.-G.; Ho, K.-C. *Angew. Chem, Int. Ed.* **2006**, *45*, 5822−5825.

(18) Chen, C.-Y.; Chen, J.-G.; Wu, S.-J.; Li, J.-Y.; Wu, C.-G.; Ho, K.-C. *Angew. Chem, Int. Ed.* **2008**, *47*, 7342−7345.

(19) Chen, C.-Y.; Wang, M.; Li, J.-Y.; Pootrakulchote, N.; Alibabaei, L.; Ngoc-le, C.-H; Decoppet, J.-D.; Tsai, J.-H.; Grätzel, C.; Wu, C.-G.; Zakeeruddin, S. M.; Grätzel, M. *ACS Nano* **2009**, *3*, 3103−3109.

(20) Gao, F.; Wang, Y.; Shi, D.; Zhang, J.; Wang, M.; Jing, X.; Humphry-Baker, R.; Wang, P.; Zakeeruddin, S. M.; Grätzel, M. *J. Am. Chem. Soc.* **2008**, *130*, 10720−10728.

(21) Gao, F.; Wang, Y.; Zhang, J.; Shi, D.; Wang, M.; Humphry-Baker, R.; Wang, P.; Zakeeruddin, S. M.; Grätzel, M. *Chem. Commun.* **2008**, 2635−2637.

(22) Cao, Y.; Bai, Y.; Yu, Q.; Cheng, Y.; Liu, S.; Shi, D.; Gao, F.; Wang, P. *J. Phys. Chem. C* **2009**, *113*, 6290−6297.

(23) Yu, Q.; Liu, S.; Zhang, M.; Cai, N.; Wang, Y.; Wang, P. *J. Phys. Chem. C* **2009**, *113*, 14559−14566.

(24) Yu, Q.; Wang, Y.; Yi, Z.; Zu, N.; Zhang, J.; Zhang, M.; Wang, P. *ACS Nano* **2010**, *4*, 6032−6038.

(25) Kim, J.-J.; Choi, H.; Kim, C.; Kang, M.-S.; Kang, H. S.; Ko, J. *Chem. Mater.* **2009**, *21*, 5719−5726.

(26) Yen, Y.-S.; Chen, Y.-C.; Hsu, Y.-C.; Chou, H.-H.; Lin, J.-T.; Yin, D.-J. *Chem.—Eur. J.* **2011**, *17*, 6781−6788.

(27) Huang, W.-K.; Cheng, C.-W.; Chang, S.-M.; Lee, Y.-P.; Diau, E. W.-G. *Chem. Commun.* **2010**, *46*, 8992−8994.

(28) Huang, W.-K.; Wu, H.-P.; Lin, P.-L.; Lee, Y.-P.; Diau, E. W.-G. *J. Phys. Chem. Lett.* **2012**, *3*, 1830−1835.

(29) Wu, K.-L.; Hsu, H.-C.; Chen, K.; Chi, Y.; Chung, M.-W.; Liu, W.-H.; Chou, P.-T. *Chem. Commun.* **2010**, *46*, 5124−5126.

(30) Chou, C.-C.; Wu, K.-L.; Chi, Y.; Hu, W.-P.; Yu, S. J.; Lee, G.-H.; Lin, C.-L.; Chou, P.-T. *Angew. Chem, Int. Ed.* **2011**, *50*, 2054−2058.

(31) Li, L.-L.; Chang, Y.-C.; Wu, H.-P.; Diau, E. W.-G. *Int. Rev. Phys. Chem.* **2012**, *31*, 420−467.

(32) Milstein, D.; Stille, J. K. *J. Am. Chem. Soc.* **1978**, *100*, 3636−3638.

(33) We have tested the photovoltaic performance of the **RD18** device with a square shadow mask of size 0.25 cm^2; the results are shown in Supplementary Figure S3. The device with a mask displays an identical V_{OC} but a lower J_{SC} than the device without a mask, leading to ∼5% reduction in power conversion efficiency. Integrating the IPCE over the AM-1.5G solar spectrum of **N719**, **RD12**, **RD16**-**RD18** (Supplementary Figure S4), and **RD18** yields a calculated J_{SC} (16.54 mA cm^{-2}) which is slightly lower than the collected value (17.80 mA cm^{-2}) obtained from the *JV* measurement.

(34) Because of the great feature for DSSC being operated under small light intensities, the stability test reported herein was performed at room temperature without imposing a strong irradiation. Under such a condition, the best performances of those devices were achieved at certain delayed times as we found in this report (e.g., 50 h for **N719**, 50−400 h for **RD12**, and 100−300 h for **RD18**).